Supplementary Material 1: Paleomagnetism and Rock Magnetism

1. Material and Methods.

General information on sample collection and preparation is presented in the main text. The magnetic mineralogy of the sediment was investigated by means of analyses of thermomagnetic curves. Representative specimens from the trimmed ends of the cores were heated in air up to 650°C in an inducing field of ~ 800 mT, using a variable field translation balance (VFTB; Krása et al., 2007). Curie temperatures of the heating cycles were determined by analyses of second-derivative curves (Tauxe, 1998) calculated with the RockMagAnalyzer software of Leonhardt (2006). The natural remanent magnetization (NRM) of the oriented specimens was investigated through stepwise thermal demagnetization up to a maximum temperature of 575 °C, with initial steps of 50 °C reduced to 25 °C from 400 °C onward. The NRM was measured after each demagnetization step using a 2-G Enterprises superconducting magnetometer placed in a shielded room. The component structure of the NRM was examined by means of vector endpoint demagnetization diagrams (Zijderveld, 1967). Magnetic components were isolated applying standard least-square analysis (Kirschvink, 1980) on linear segments of the demagnetization paths. Mean directions and associated statistic parameters were calculated using the spherical statistic of Fisher (1953). Directional analyses were performed with the PaleoMag software of Jones (2002). All the analyses were conducted at the paleomagnetic laboratory of the Ludwig-Maximilian University (Munich, Germany).

2. Results.

The heating cycle of the thermomagnetic curves from all sites (except for the Patrignone Creek section) is characterized by a decrease of magnetization up to ~ 575°C, which is the Curie temperature of magnetite (Fig. 1a-c). This decay is interrupted by a smooth increase of magnetization that peaks at ~ 500 °C, not visible in the cooling cycle. Similar behavior has been observed in sediments containing ferriferous phases like pyrite, siderite, and Fe-enriched smectite (Hirt and Gehring, 1991; Hirt et al., 1993; Passier et al., 2001; Dallanave et al., 2015). In the specimen from the Patrignone Creek section (Fig. 1d) the magnetic phase appears to be dominated by greigite; the minimum of magnetization between 300 °C and 400 °C is a common feature of thermomagnetic experiments of samples containing greigite, which irreversibly breaks down during heating above ~ 280 °C (Roberts, 1995; Roberts et al., 2011). This decay is followed by a marked peak of magnetization at ~ 500 °C, indicating the

formation of magnetite from the greigite precursor (e.g., Roberts et al., 2011). Magnetite is then the dominant mineral during the cooling cycle, which back at room temperature shows a magnetization ~ 6 times higher than before thermal treatment.

The intensity of the NRM varies widely between the sites. The highest values are observed at Bulera, with an average initial magnetization of the samples of 1.89 Am^{-1}, while the minimum average value of 4.14 $x10^{-5}$ Am^{-1} is observed at Cava Gosti, where, however, no suitable magnetic directions were isolated. The average intensity NRM of all the samples is 0.4 Am^{-1}. Scattered magnetic component directions are observed between room temperature and generally 150–300 °C. Characteristic magnetic component (ChRM) directions linearly trending to the origin of the demagnetization axes were isolate in 66% ($^{97}/_{148}$) of the samples generally up to 450–550°C (Fig. 2a-i). The lowest ChRM component unblocking temperatures (300–350°C) have been observed at Magliano and Patrignone Creek sections (Fig. 2j). These data, together with the thermomagnetic remanence curves described above, reveal that the primary magnetization is generally carried by magnetite except at Magliano and Patrignone Creek, where greigite is the dominant magnetic phase. Of the 11 sampling sites where ChRM directions were isolated, 6 are characterized by the presence of directions pointing North-and-down, 3 of directions pointing South-and-up, while 2 of directions pointing in both the modes (Fig. 3a-k). We calculated the mean ChRM direction for all sites before and after correction for bedding tilt if present; for Poggio del Gallo and Casciana Terme, we calculated the mean ChRM direction for both the N-and-down and S-and-up modes. We calculated the statistical parameter of Fisher (1953) associated to each mean ChRM direction except at Montegabbro and Pescille, where only 2 directions were available. The results are shown in Fig. 3a-k and listed in Table 1. We plotted all the site-mean directions (Fig. 3l) and we calculated the average direction of both the N-and-down and S-and-up modes (Table 1). They depart from antipodality by 7.1°, passing the reversal test with class "B" of McFadden and McElhinny (1990).

For each site, we calculated the position of the virtual geomagnetic pole (VGP) associated to each ChRM direction. We interpreted the magnetic-polarity stratigraphy using the latitude of each VGP relative to the mean paleomagnetic north pole (Kent et al., 1995; Lowrie and Alvarez, 1977). VGP relative latitudes approaching +90° or -90° N are interpreted as recording normal or reverse polarity, respectively. Results are shown in Fig. 4. The detailed chronostratigraphic correlation of each site is described in Table 3 of the main text.

Figure Captions

Figure 1. Representative thermomagnetic curves of specimens from Bulera (bp05), Pescille (pp04), Roccastrada (rp02), and Patrignone Creek sections (mp03); M = magnetization. Insets show second derivative-curves of the heating cycles between 500 and 700 °C, used to estimate the Curie temperature of the magnetic phase. Only thermomagnetic curves b) and c) are corrected for a diamagnetic component due to the high carbonate concentration in the sediment.

Figure 2. Representative vector end-point demagnetization diagrams of thermally demagnetized core specimens from different sites. **A**) Bulera, sample bp09; **B**) Colombaio, sample cp02; **C**) Montefollonico, sample mfp05; **D**) Montegabbro, sample mgp02; **E**) Pescille, sample pps03; **F**) Cetona–Poggio del Gallo, sample pgp17; **G**) Pianosa, sample pm05; **H**) Casciana Terme, sample pp01; **I**) Roccastrada, sample rp03; **J**) Patrignone Creek, sample mp04a). Closed (open) squares represent vector end points projection onto horizontal (vertical) plane. Dashed lines highlight the ChRM directions trending to the origin of the demagnetization axes.

Figure 3. **A**-**K**) Tilt-corrected equal area projection of the ChRM directions for each site; filled (open) squares represent down (up) pointing ChRM directions; filled (open) circles are the down (up) pointing mean ChRM directions with associated α_{95} (gray circle). The α_{95} parameter has not been calculated for sites with 2 ChRM directions. **L**) Tilt-corrected equal area projection of the N-and-down (filled squares) and S-and-up (open squares) mean ChRM directions from all sites, with the average direction calculated for both the modes (filled and open circles) and the associated α_{95}; the closed diamond is the all-sites mean direction calculated inverting all site-means to a common North pointing polarity, shown with the associated α_{95}.

Figure 4. Virtual geomagnetic pole (VGP) latitude calculated from the ChRM direction of each site, plotted *vs*. the stratigraphic position of the samples. The relative latitude of the poles was used to interpret the magnetic polarity (MP): black (white) bars indicate normal (reverse) polarity. Gray bars represent intervals where no suitable magnetic directions were isolated.

Table 1. Characteristic component mean directions.
Bedding = strike and dip of the sampled strata (°); N = number of samples (* = number of site means); MAD = average maximum angular deviation (°); k = Fisher precision parameters; α_{95} = Fisher radius of cone of 95% confidence; Dec and Inc =

declination and inclination (°); NPD = normal polarity (north-and-down pointing) directions; RPD = reverse polarity (south-and-up pointing) directions.

References

DALLANAVE, E., AGNINI, C., BACHTADSE, V., MUTTONI, G., CRAMPTON, J.S., STRONG, C.P., HINES, B.R., HOLLIS, C.J., AND SLOTNICK, B.S., 2015, Early to middle Eocene magneto-biochronology of the southwest Pacific Ocean and climate influence on sedimentation: Insights from the Mead Stream section, New Zealand: Geological Society of America, Bulletin, v. 127, p. 643–660.

FISHER, R., 1953, Dispersion on a sphere: Royal Society of London, Proceedings, v. A217, p. 295–305.

HIRT, A.M., AND GEHRING, A.U., 1991, Thermal Alteration of the Magnetic Mineralogy in Ferriginous Rocks: Journal of Geophysical Research, v. 96, p. 9947–9953.

HIRT, A.M., BANIN, A., AND GEHRING, A.U., 1993, Thermal generation of ferromagnetic minerals from iron-enriched smectites: Geophysical Journal International, v. 115, p. 1161–1168.

JONES, C.H., 2002, User-driven integrated software lives: "Paleomag" paleomagnetics analysis on the Macintosh: Computer & Geosciences, v. 28, p. 1145–1151.

KENT, D. V., OLSEN, P.E., AND WITTE, W.K., 1995, Late Triassic-earliest Jurassic geomagnetic polarity sequence and paleolatitudes from drill cores in the Newark rift basin, eastern North America: Journal of Geophysical Research, v. 100, p. 14,965–14,998.

KIRSCHVINK, J.L., 1980, The least-squares line and plane and the analysis of palaeomagnetic data: Geophysical Journal of the Royal Astronomical Society, v. 62, p. 699–718.

KRÁSA, D., PETERSEN, K., AND PETERSEN, N., 2007, Variable field translation balance, *in* Gubbins, D., and Herrero-Bervera, E., eds., Encyclopedia of Geomagnetism and Paleomagnetism: Berlin, Springer, p. 977–979.

LEONHARDT, R., 2006, Analyzing rock magnetic measurements: The RockMagAnalyzer 1.0 software: Computer & Geoscience, v. 32, p. 1420–1431.

LOWRIE, W., AND ALVAREZ, W., 1977, Upper Cretaceous–Paleocene magnetic stratigraphy at Gubbio, Italy: III. Magnetic stratigraphy: Geological Society of America, Bulletin, v. 88, p. 374–377.

MCFADDEN, P.L., AND MCELHINNY, M.W., 1990, Classification of the reversal test in palaeomagnetism: Geophysical Journal International, v. 103, p. 725–729.

PASSIER, H.F., DE LANGE, G.J., AND DEKKERS, M.J., 2001, Magnetic properties and geochemistry of the active oxidation front and the youngest sapropel in the eastern Mediterranean Sea: Geophysical Journal International, v. 145, p. 604–614.

ROBERTS, A.P., 1995, Magnetic properties of sedimentary greigite (Fe_3S_4): Earth and Planetary Science Letters, v. 134, p. 227–236.

ROBERTS, A.P., CHANG, L., ROWAN, C.J., HORNG, C.S., AND FLORINDO, F., 2011, Magnetic properties of sedimentary greigite (Fe_3S_4): An update: Review of Geophysics, v. 49, p. RG1002.

TAUXE, L., 1998, Paleomagnetic Principles and Practice: Dordrecht, The Netherlands, 299 p.

ZIJDERVELD, J.D.A., 1967, A.C. demagnetization of rocks: analysis of results, *in* Collinson, D.W., Creer, K.M., and Runcorn, S.K., eds., Methods in Paleomagnetism: New York, Elsevier, p. 254–286.

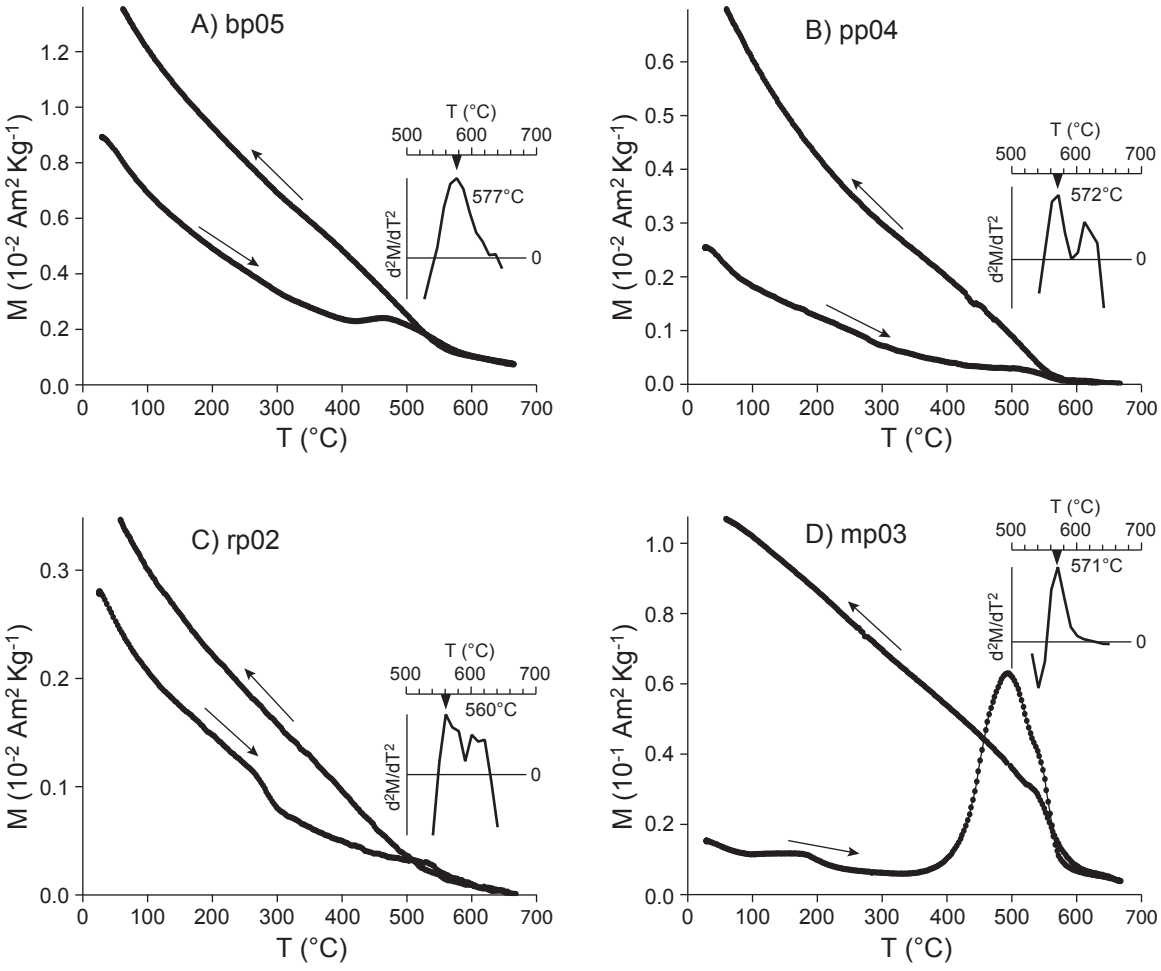
A) bp05
M (10-2 Am2 Kg-1)
T (°C)
577°C
d2M/dT2
B) pp04
572°C
C) rp02
560°C
D) mp03
M (10-1 Am2 Kg-1)
571°C

Figure 1

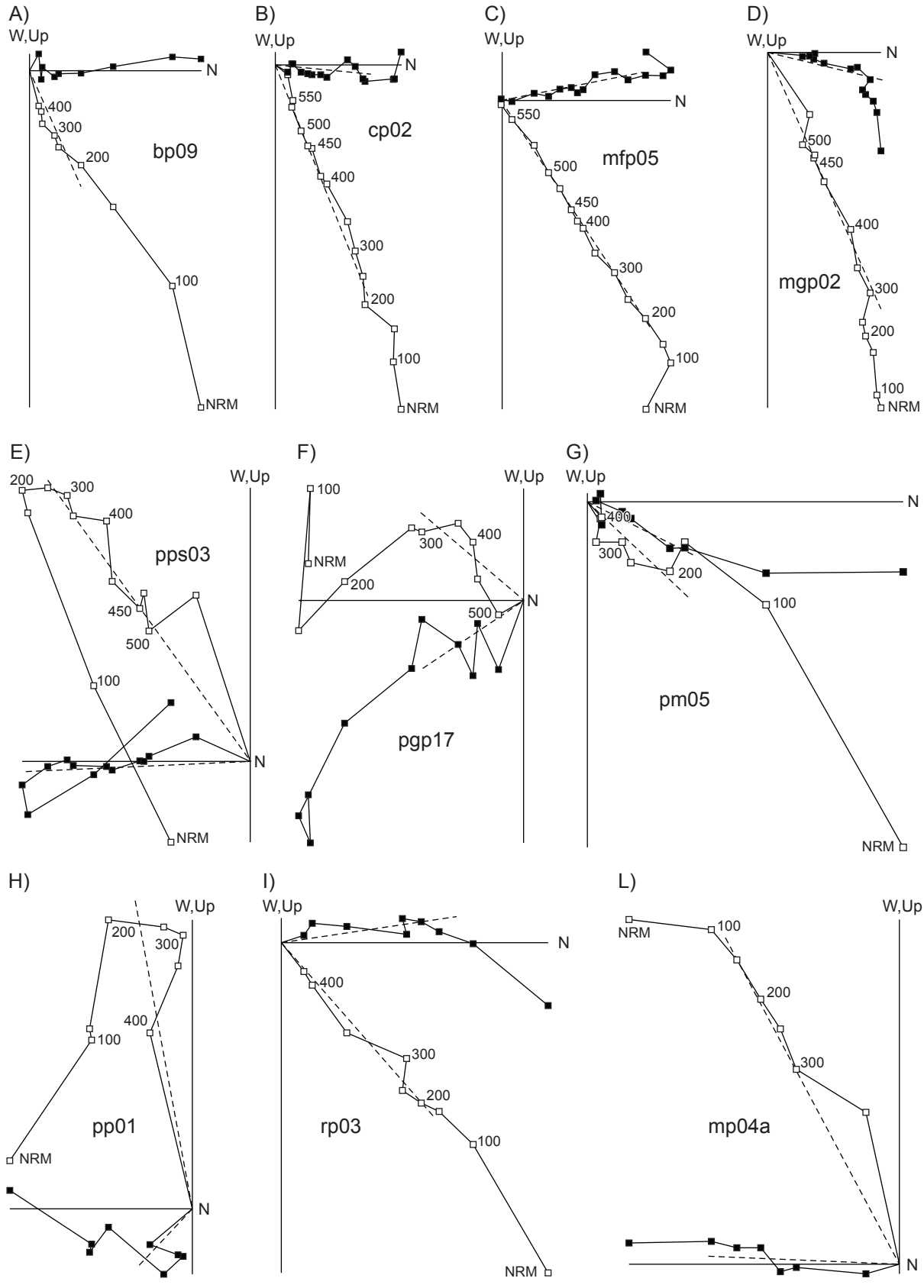
A)
W,Up
N
400
300
200
bp09
100
NRM
B)
W,Up
N
550
500
450
cp02
400
300
200
100
NRM
C)
W,Up
N
550
500
mfp05
450
400
300
200
100
NRM
D)
W,Up
N
500
450
400
mgp02
300
200
100
NRM
E)
200
300
400
W,Up
pps03
450
500
100
N
NRM
F)
100
W,Up
NRM
300
400
200
N
500
pgp17
G)
W,Up
N
400
300
200
100
pm05
NRM
H)
W,Up
200
300
400
100
pp01
NRM
N
I)
W,Up
N
400
300
200
rp03
100
NRM
L)
W,Up
NRM
100
200
300
mp04a
N

Figure 2

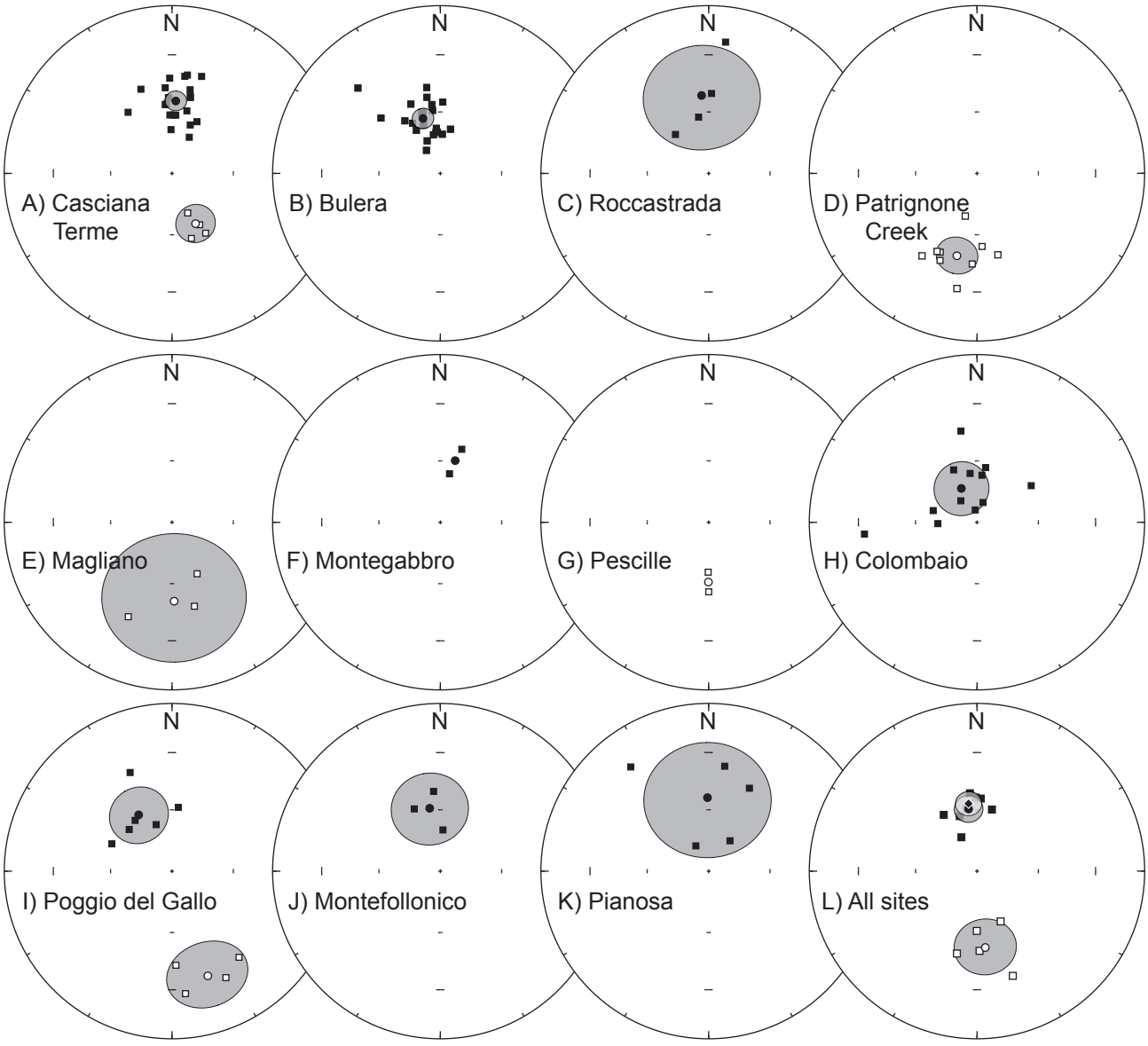
N
A) Casciana Terme
B) Bulera
C) Roccastrada
D) Patrignone Creek
E) Magliano
F) Montegabbro
G) Pescille
H) Colombaio
I) Poggio del Gallo
J) Montefollonico
K) Pianosa
L) All sites

Figure 3

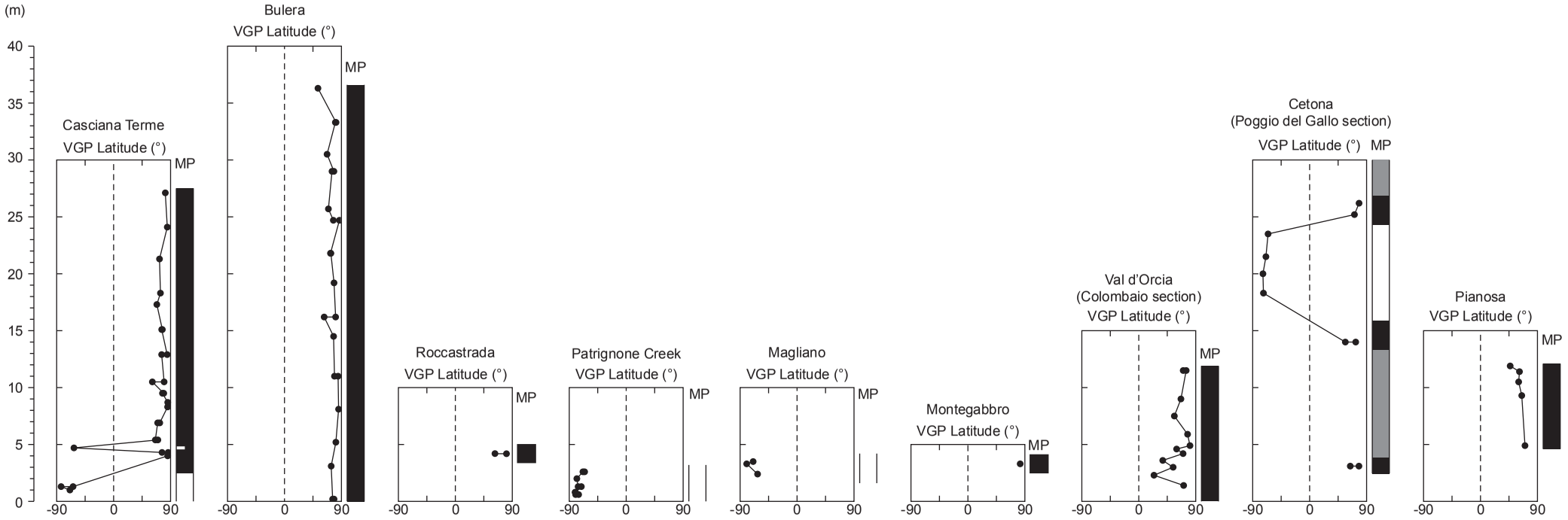
(m)
40
35
30
25
20
15
10
5
0
Casciana Terme
VGP Latitude (°)
MP
Bulera
VGP Latitude (°)
MP
Roccastrada
VGP Latitude (°)
MP
Patrignone Creek
VGP Latitude (°)
MP
Magliano
VGP Latitude (°)
MP
Montegabbro
VGP Latitude (°)
MP
Val d'Orcia
(Colombaio section)
VGP Latitude (°)
MP
Cetona
(Poggio del Gallo section)
VGP Latitude (°)
MP
Pianosa
VGP Latitude (°)
MP
-90
0
90

Figure 4

Table 1. Characteristic component mean directions

				Geographic coordinates				Tilt corrected coordinates			
Site	Bedding	N	MAD	κ	α_{95}	Dec	Inc	κ	α_{95}	Dec	Inc
Bulera	167/8	22	4.3	38.1	5.1	357.6	61.3	38.4	5.1	342.5	61.9
Poggio del Gallo (NPD)	198/10	6	8.0	25.9	12.2	344.9	65.3	20.0	13.9	329.4	58.0
Poggio del Gallo (RPD)	198/10	4	13.9	25.7	15.9	165.8	-34.3	20.78	17.8	161.1	-34.4
Val d'Orcia	0/0	12	5.4	10.8	13.2	335.2	71.9	10.8	13.2	335.2	71.9
Patrignone Creek	22/13	9	8.3	29.8	9.6	184.6	-48.7	30.1	9.5	193.7	-48.1
Magliano Paese	0/0	3	8.1	9.7	33.0	178.2	-50.7	9.7	33.0	178.2	-50.7
Montefollonico	162/8	3	3.8	31.2	18.2	3.4	57.5	31.2	18.2	350.7	59.6
Monte Gabbro	0/0	2	2.5	---	---	13.6	59.0	---	---	13.6	59.0
Casciana (NPD)	285/15	21	5.5	60.7	4.1	359.9	62.7	42.0	4.9	3.0	54.3
Casciana (RPD)	285/15	4	16.1	26.1	15.8	134.2	-70.2	72.6	9.38	154.8	-62.9
Pescille	0/0	2	3.8	---	---	180.2	-60.8	---	---	180.2	-60.8
Pianosa	0/0	5	12.3	6.1	29.6	359.1	53.9	6.1	29.6	359.1	53.9
Roccastrada	10/10	4	7.3	9.4	27.0	343.7	47.9	9.4	27.0	354.8	51.5
All Sites (NPD)	---	8*	---	72.6	6.5	355.3	60.2	69.7	6.7	352.3	59.3
All Sites (RPD)	---	5*	---	23.5	16.1	171.7	-53.9	29.8	14.3	173.8	-52.2
All Sites (N+R)	---	13*	---	41.8	6.5	353.8	57.8	46.4	6.1	352.9	56.6